Int J Adv Manuf Technol (2016) 82:143–152
DOI 10.1007/s00170-015-7346-1

ORIGINAL ARTICLE

Analysis of tool-particle interactions during cutting process of metal matrix composites

A. Ghandehariun[1] · H. A. Kishawy[1] · U. Umer[2] · H. M. Hussein[2,3]

Received: 17 March 2015 / Accepted: 19 May 2015 / Published online: 7 June 2015

Abstract Metal matrix composites (MMCs) have become common materials that are employed in different industrial applications due to their outstanding strength and wear resistance. However, machining MMCs is considered to be a challenging process. This paper presents a micro-mechanical finite element analysis developed for simulation of MMC machining. Unlike the previously developed FE models, this model simulates the behavior of all main components that distinguish the MMC, namely the matrix, particles, and the particle-matrix interface, during the process. As a result, various aspects of the process, such as debonding and fracture in the particles and different scenarios of tool-particle interactions can be studied using the proposed model. The predicted forces were compared to the measured ones and used to verify the presented model. The developed model is successful in providing a broad understanding of MMC machining process.

Keywords Metal matrix composites (MMCs) · Finite element analysis (FEA) · Machining · Debonding

✉ A. Ghandehariun
Amirmohammad.Ghandehariun@uoit.ca

[1] Machining Research Laboratory (MRL), Faculty of Engineering and Applied Science, University of Ontario Institute of Technology (UOIT), Oshawa, ON, Canada

[2] Advanced Manufacturing Institute, King Saud University, Riyadh 11421, Saudi Arabia

[3] Present address: Faculty of Engineering, Helwan University, Helwan, Egypt

1 Introduction

Composite materials are defined as a combination of various substances with different chemical and mechanical properties that will not dissolve in each other. The matrix phase transfers load and supports the integrity of the structure, while the particle phase provides the enhanced composite characteristics. Among various types of composite materials, metal matrix composites (MMCs) have become common materials that are employed in many industrial applications due to their outstanding strength and wear resistance [1]. Examples of MMC applications include cylinder liners for internal combustion engines, modern landing gears, ventral fins in fighter planes and helicopter blades [2]. Even though near net shape manufacturing is usual for composites, machining processes are generally required for achieving the desired characteristics on the final product [3, 4].

Existence of ceramic reinforcements in MMCs has its own drawbacks; the reinforcing phases in these composites have characteristics that are similar to those of the cutting tool materials. Consequently, machining MMCs can result in excessive tool wear, which in turn causes various types of damage in the machined product. Thus, machining MMCs is considered to be a challenging process. In order to have a better control over the MMC machining surface quality, it has become clear that a comprehensive understanding of the behavior of MMC materials during machining is required. Knowledge related to the deformation mechanism of MMC during machining is needed in order to attain the optimal process.

Various approaches were used for studying the MMC machining process [5, 6]. The numerical simulations approached the problem at two levels; macro-mechanical models simulated the cutting process by treating the material as a macroscopically anisotropic material, while micro-mechanical models focused on the interaction between particles and matrix.

Macroscopic models often disregard many fundamental characteristics of the composite material and cannot determine the details of material behavior. Microscopic models usually provide more details of the actual behavior of the matrix as well as particle interaction with the tool during the cutting process and offer a more realistic simulation of the interaction between the tool and composite material.

An early model for predicting cutting forces during machining MMCs was presented by Kishawy et al. [7]. In their research, an analytical force model for orthogonal cutting was provided based on the total energy required for the cutting process. Sikder and Kishawy [8] presented another analytical force model for calculation of cutting forces during MMC machining which considered several characteristics of the cutting process, such as shear force, ploughing force, and particle fracture force. Kishawy et al. [9] also proposed a model for predicting tool wear during machining of MMC materials. Their model took into account the effects of various types of abrasion on the cutting tool in order to calculate the flank wear.

An analysis of characteristics of machined surface of MMCs was performed by Kannan and Kishawy [10]. Their research investigated the variations of microhardness beneath the machined surface and provided an understanding of the effects of machining parameters and MMC properties on the quality of the surface.

The new improvements in computer technologies have empowered researchers to gain a better understanding of the cutting process through complex numerical simulations. Finite element modeling is a major numerical technique utilized by many researchers in this field [11–14].

Zhu and Kishawy [15] provided a thermo-mechanical finite element analysis for the MMC cutting process. Their finite element model managed to predict the cutting forces as well as the distribution of stress and temperature in the workpiece material. Later, Pramanik et al. [16] provided a basic investigation of the tool-particle interactions during MMC orthogonal cutting using finite element methods. A more recent finite element investigation of the MMC cutting process was conducted by Zhou et al. [17]. This research work provided a two-dimensional thermo-mechanical model of orthogonal cutting which is utilized in analysis of the removal mechanism of the particle from the matrix. Dandekar and Shin [18] provided a multistep 3D model for prediction of subsurface damage during the MMC machining process. They initially simulated the process using a single-phase equivalent homogenous material (EHM) model and then applied the obtained data to a local multiphase model. This model provided a better prediction of debonding and particle fracture as well as the depth of damage in the composite material during the cutting process. Wang et al. [19] presented a simulation of formation of defects during machining aluminum MMCs with high volume fraction of particles. Their study considered fracture in particles, though failed to account for the role of particle debonding in formation of defects on MMC machined surface. Nevertheless, none of the currently available finite element models for MMC machining are able to simulate the cutting and chip formation process on the actual three-phase composite material.

This paper presents a novel micro-mechanical finite element (FE) model of MMC cutting process. Model predictions are validated by means of comparison with experimentally measured data. This model contributes to the knowledge regarding machining MMCs through simulation of the behavior of all phases of the composite, namely matrix, particle, and particle-matrix interface, during cutting. This distinguishes the developed model from the previously developed MMC cutting FE models. Detailed modeling of the distinct phases of the MMC workpiece enables the presented FE simulation to provide a more comprehensive understanding of the behavior of the composite material during machining.

Investigation of interactions between the cutting tool and reinforcements is an important part of understanding MMC machining. These interactions can cause fluctuations in the cutting force, deterioration of machined surface quality, and decline in the life of cutting tool. Tool-particle interactions during MMC cutting can lead to cases of particle fracture, particle debonding, or particle squeeze into matrix material. The available literature, such as the model presented in [20], does not offer a broad knowledge about this area, as the models used in investigations could not provide a through simulation of MMC behavior. On the other hand, the presented model is capable of being utilized for analysis of all the interactions between the cutting tool and particles.

2 Finite element model of the process

2.1 Problem description

Two-dimensional finite element modeling is performed for simulation of orthogonal cutting of an aluminum MMC. Workpiece material parameters are provided in Table 1. Simulation is performed in Abaqus/Explicit environment. Lagrangian modeling is employed as, unlike other types of analysis, it permits modeling the behavior of nonplastic reinforcements as well as their interactions with the plastic matrix.

Table 1 Workpiece material parameters

Matrix material	Aluminum Al6061
Particle material	Alumina (Al_2O_3)
Particle volume fraction	10 %
Average particle diameter	15 μm

Table 2 Cutting parameters for the analysis

Rake angle	30°
Clearance angle	3°
Cutting speed	85 m min^{-1}
Depth of cut	0.1 mm
Width of cut	3 mm

Cutting process is performed using a tungsten carbide cutting tool, and the cutting edge is assumed to be ideally sharp. Tool geometry and cutting parameters used in analysis of the process are listed in Table 2.

The analysis utilizes an elastic material model for the tool. The behavior of the three phases of the composite material is simulated. Matrix and particles are modeled as thermal-elastic-plastic materials using quad thermal-displacement plain strain elements. The particle-matrix interface is modeled using cohesive zone elements which are appropriate options for modeling the interface with very small thickness.

The interface elements are tied to both matrix and particle surfaces. A sacrificial layer of elements is defined along the cutting path in order to simulate chip separation using progressive damage model. This layer consists of elements which will be deleted as soon as damage accumulation in the material reaches the maximum value and material fracture occurs.

Contact is defined between rake and flank surfaces of the tool and workpiece surfaces as well as the tool surfaces and the particle nodes. This will enable the model to simulate tool-particle interactions. The extended Coulomb friction model [21] is used in contact definitions. This model represents the frictional stress in two distinct regions of sticking and sliding:

$$\begin{cases} \tau_f = \mu\sigma_n & \text{when } \mu\sigma_n < \tau_{max} \\ \tau_f = \tau_{max} & \text{when } \mu\sigma_n \geq \tau_{max} \end{cases} \quad (1)$$

In Eq. (1), τ_f is the frictional shear stress on the surface, σ_n is the normal stress, μ is the coefficient of friction, and τ_{max} is the maximum possible shear stress on the interface. In this research, τ_{max} is assumed to be equal to $\sigma_y/\sqrt{3}$ where σ_y is the yield stress of the matrix material. This value is considered as a reasonable upper bound estimate for the maximum shear stress on the interface [22].

2.2 Material modeling

2.2.1 Matrix material

Matrix material is modeled using a thermal-elastic-plastic constitutive equation until fracture. Johnson-Cook plasticity model [23] is employed for simulation of matrix material behavior. This is one of the more commonly used constitutive models for simulating materials subjected to large strains, high strain rates, and high temperatures, which are common characteristics of the cutting process. The basic form of Johnson-Cook model for the von Mises flow stress, σ, is provided in the following equation [23]:

$$\sigma = (A + B\epsilon^n)\left[1 + C\ln\left(\frac{\dot{\epsilon}}{\dot{\epsilon}_0}\right)\right]\left[1-\left(\frac{T-T_{\text{transition}}}{T_{\text{melt}}-T_{\text{transition}}}\right)^m\right] \quad (2)$$

In Eq. (2), ϵ is the equivalent plastic strain, $\dot{\epsilon}$ is the plastic strain rate, and $\dot{\epsilon}_0$ is the reference strain rate. T and T_{melt} are the current temperature and the material melting temperature, respectively. $T_{\text{transition}}$ is the transition temperature defined as the temperature below which material behavior will have no temperature dependence. The five material constants, namely A, B, C, n, and m, are obtained using torsion tests, static tensile tests, and dynamic Hopkinson bar tensile tests for various materials.

Chip formation is simulated using element deletion in the sacrificial layer of elements. Element deletion is modeled using Johnson-Cook's model for progressive damage and fracture [24]. According to this model, damage in an element is defined as

$$D = \sum \frac{\Delta\epsilon}{\epsilon^f} \quad (3)$$

where $\Delta\epsilon$ is the change in the equivalent plastic strain during each integration cycle and ϵ^f is the equivalent strain to fracture as a function of temperature, strain rate, equivalent stress, and pressure. D is a parameter for quantifying damage in the element, and fracture will occur when D=1.0.

The strain to fracture can be calculated according to the following expression [24]:

$$\epsilon^f = \left[D_1 + D_2\exp(D_3\sigma^*)\right]\left[1 + D_4\ln\left(\frac{\dot{\epsilon}}{\dot{\epsilon}_0}\right)\right]\left[1 + D_5\left(\frac{T-T_{\text{transition}}}{T_{\text{melt}}-T_{\text{transition}}}\right)\right] \quad (4)$$

In Eq. (4), σ^* is the dimensionless pressure-stress ratio (stress triaxiality) defined as $\sigma^* = \sigma_m/\overline{\sigma}$ where σ_m is the average of three normal stresses and $\overline{\sigma}$ is the von Mises equivalent stress. $D_1 \ldots D_5$ are material constants which can be obtained using the aforementioned materials tests. Matrix and cutting tool material properties are provided in Table 3.

Table 3 Material properties for Al6061 aluminum matrix and tungsten carbide cutting tool

Tool modulus of elasticity (GPa) [25]	668.35
Tool Poisson's ratio [25]	0.24
Tool conductivity (W m^{-1} K^{-1}) [25]	173
Tool specific heat (J kg^{-1} K^{-1}) [25]	250
Matrix modulus of elasticity (GPa) [26]	68.9
Matrix Poisson's ratio [26]	0.33
Matrix conductivity (W m^{-1} K^{-1}) [26]	167
Matrix specific heat (J kg^{-1} K^{-1}) [26]	896
Johnson-Cook model parameters [27]	
A (MPa)	324
B (MPa)	114
C	0.002
n	0.42
m	1.34
T_{melt} (°C)	582
$T_{transition}$ (°C)	20
ϵ_0	1.0
D_1	−0.77
D_2	1.45
D_3	−0.47
D_4	0.0
D_5	1.60

2.2.2 Particle material

The alumina particles are modeled as perfectly elastic materials until failure. Particle fracture simulation is performed using the brittle cracking model. Particle material properties are provided in Table 4.

2.2.3 Particle-matrix interface

The interface between the particles and matrix in the workpiece material is modeled using cohesive zone elements. Formulation of cohesive zone elements for utilization in finite element models is provided by Foulk et al. [29]. This type of elements has been used by Tvergaard [30] for simulation of debonding in the fiber-matrix interface in a whisker-reinforced aluminum metal matrix composite.

The particle-matrix interface in the current analysis is modeled using a traction-separation law. Damage initiation in the interface is predicted using quadratic nominal stress criterion. According to this criterion, damage in the cohesive elements is initiated when the following quadratic interaction condition is satisfied [31]:

$$\left\{\frac{\langle t_n\rangle}{t_n^o}\right\}^2+\left\{\frac{t_s}{t_s^o}\right\}^2+\left\{\frac{t_t}{t_t^o}\right\}^2=1 \tag{5}$$

In Eq. (5), t_n, t_s, and t_t are the normal, first direction shear, and second direction shear (in a three-dimensional problem) of the traction stress vector, respectively. t_n^o, t_s^o, and t_t^o represent the maximum nominal normal, first direction shear, or second direction shear stress. The brackets <> demonstrate that a pure compressive stress cannot initiate damage.

The progressive evolution of damage, which will result in failure of the cohesive element and its deletion, is modeled using the energy approach. In this approach, the energy dissipated as a result of damage in the element until failure is a prescribed value. This value is entered into the model as a material property. This property is equal to the area under the traction-separation curve. Element will be deleted after the dissipated energy reaches the failure energy property. The interfacial failure energy (Φ) for the Al/Al_2O_3 interface is selected as Φ=50 J/m^2. This value is similar to the value used for simulation of damage in interface elements by Dandekar and Shin [18].

2.3 Meshing

The matrix and the particle phases of the workpiece are meshed using quad thermal-displacement plane strain elements. Similar elements are used for the cutting tool. For these phases, free meshing technique is used. Meshing of the particle-matrix interface is performed using zero thickness cohesive zone elements.

Dependence of the model results on the element size is investigated by comparing the cutting forces obtained from models with different mesh seeds. The average node distances in different parts of the optimum mesh for the

Table 4 Material properties for alumina particles

Flexural strength (MPa)	380
Conductivity (W m^{-1} K^{-1})	33
Elastic modulus (GPa)	416
Poisson's ratio	0.231
Coefficient of thermal expansion (K^{-1})	4.6×10^{-6}
Specific heat (J kg^{-1} K^{-1})	755

From Munro [28]

Table 5 Average node distance in the optimum mesh

	Average node distance
Edge of particles along the cutting line	2.00 μm
Edge of particles above the cutting line	2.36 μm
Edge of particles below the cutting line	2.36 μm
Matrix along the cutting line	4.00 μm
Matrix above the cutting line	4.43 μm
Matrix at the bottom	10.00 μm
Cohesive particle-matrix interface	0.48 μm

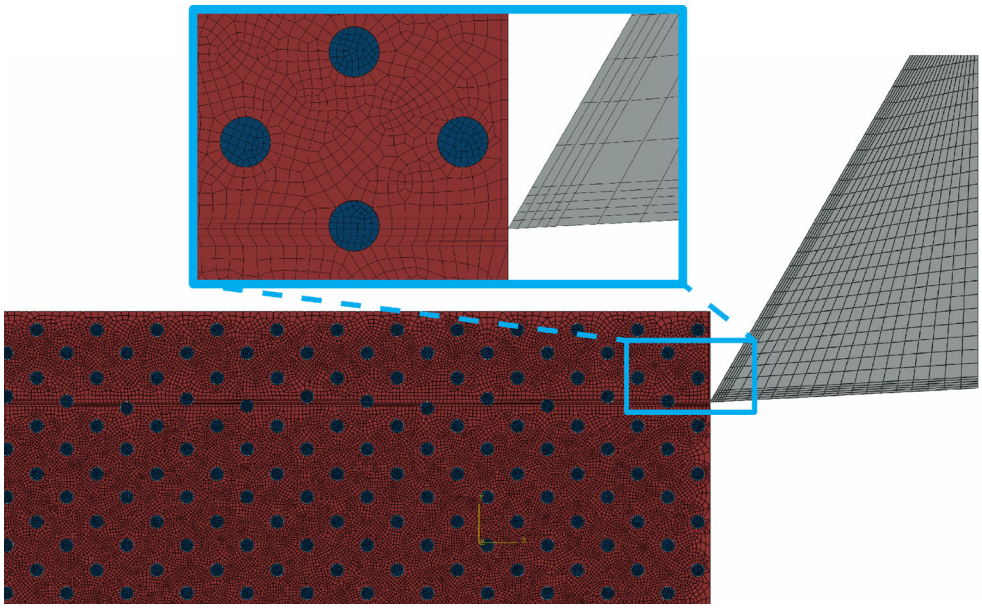

Fig. 1 Meshed parts for the finite element analysis

model are detailed in Table 5. The meshed parts for the model are shown in Fig. 1.

3 Results and discussion

The solution of the finite element model is performed using Abaqus to obtain the distribution of various parameters in the model. Validation of the model results is the first step in analysis of the model outputs.

3.1 Model validation

In order to validate the results of the finite element model, the obtained predicted values of the cutting force were compared with the experimental results from cutting tests performed under the same cutting conditions [15]. Comparison of the average cutting force during the steady phase of cutting process from the FEM and the one obtained in experiments is provided in Fig. 2. As can be seen in this figure, the value of the cutting force obtained in simulations is within the standard deviation error range of the experimental value. The difference between the average simulated and experimental values is 8.3 %.

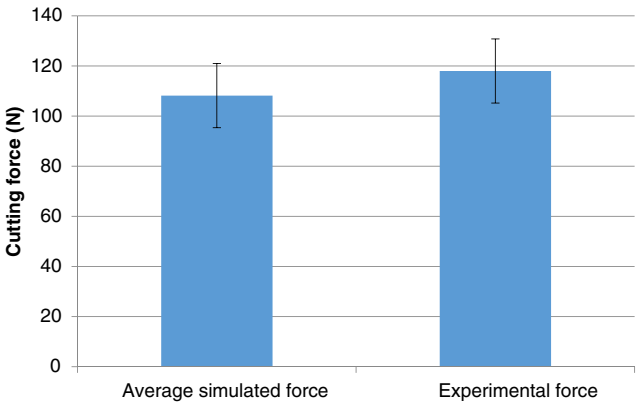

Fig. 2 Comparison of cutting forces obtained using FEM and experimental data [15] (Al 6061/10 % 15 μm Al_2O_3, v=85 m/min, rake angle=30°, width of cut=3 mm)

Figure 2 shows that the simulated cutting force is slightly smaller than the experimental force. This is expected in the finite element model since the cutting tool was assumed to be ideally sharp in the analysis, which is not the case in the actual machining tests. Even if the cutting tool is sharp at the beginning of the cut, the tool wear around the cutting edge will soon increase the cutting edge radius and thus the cutting force.

3.2 Analysis of cutting force during machining

Figure 3 shows the cutting force versus time obtained during finite element simulation of the steady phase of cutting process. Apparent in this figure are the peaks and troughs in the cutting force which are associated with the interactions between the cutting tool and reinforcements. It is evident from this figure that initiation and progress of crack in the particle can cause a decrease in the cutting force. On the other hand, interaction of the particle with the cutting tool before initiation of crack results in an increase of the cutting force.

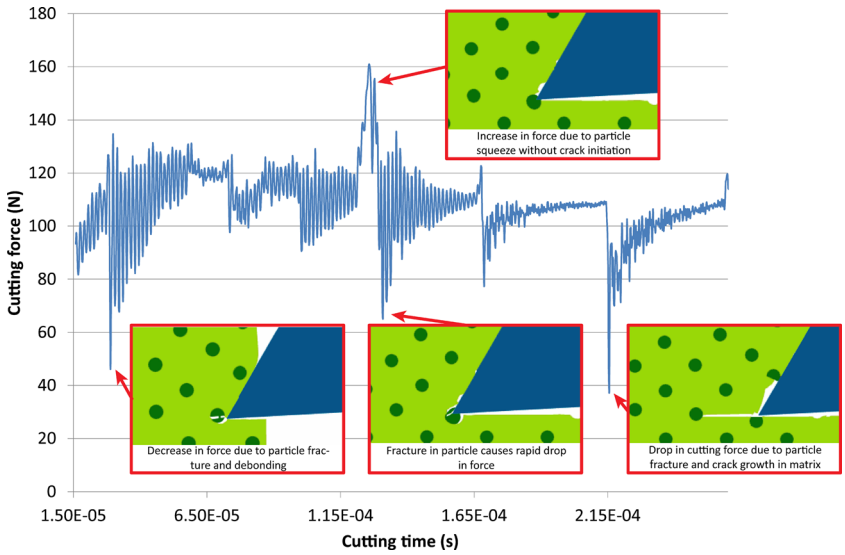

Fig. 3 Cutting forces obtained using finite element analysis (Al 6061/10 % 15 μm Al_2O_3, v= 85 m/min, rake angle=30°, width of cut=3 mm)

3.3 Tool-particle interaction scenarios

The presented FE analysis in this research is unique in terms of simulating the cutting process on the real composite material with all its phases; this is in contrast to the models available in the literature where either a simplified composite model (i.e., without modeling the interface) [16] or an equivalent homogeneous material (EHM) model [18] is used for simulation of MMC machining. Utilization of a comprehensive model for MMC behavior during cutting enables the FE analysis to predict fracture and debonding in the reinforcements. This ability makes the developed FE model an appropriate tool for studying various interaction scenarios between the tool and particles.

In this paper, interactions between the tool and particles are studied for the particles along the cutting path. Different cases of particle fracture and debonding can occur as the cutting tool approaches the particles. The main three scenarios for particles located along, above, and below cutting line are depicted in Fig. 4. These cases will be analyzed in this section.

Figure 5a shows the engagement of the cutting tool and a particle located along the cutting line. The cutting line passes through the central area of the particle. It is clear that as a result of engagement between the tool and the particle, the energy level has reached the critical value which is shown as deletion of cohesive interface elements. This indicates that debonding has started.

It is also apparent from Fig. 5a that debonding of the particle initiated before any contact with the tool. This can be

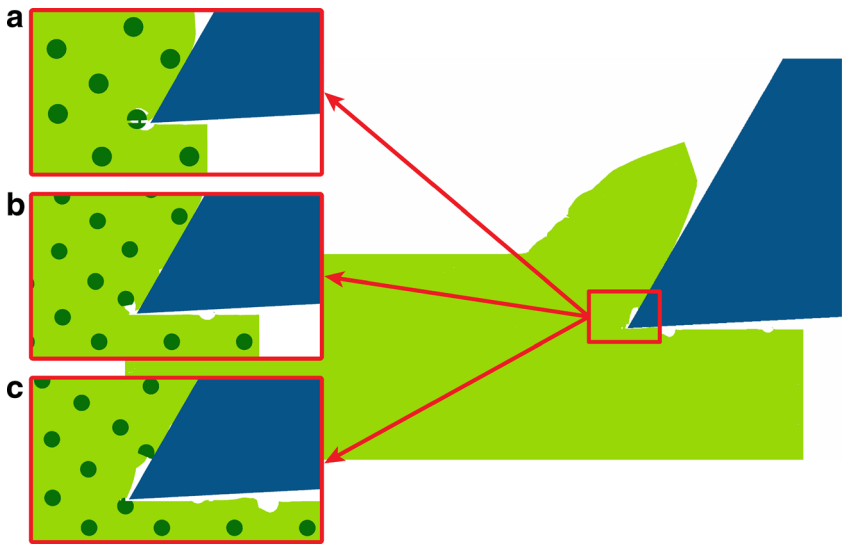

Fig. 4 Different scenarios of tool-particle interactions at three different time steps: **a** particle on the cutting line, fractured and debonded; **b** particle above the cutting line, pushed in the chip; and **c** particle below cutting line, fractured and attached to the machined surface

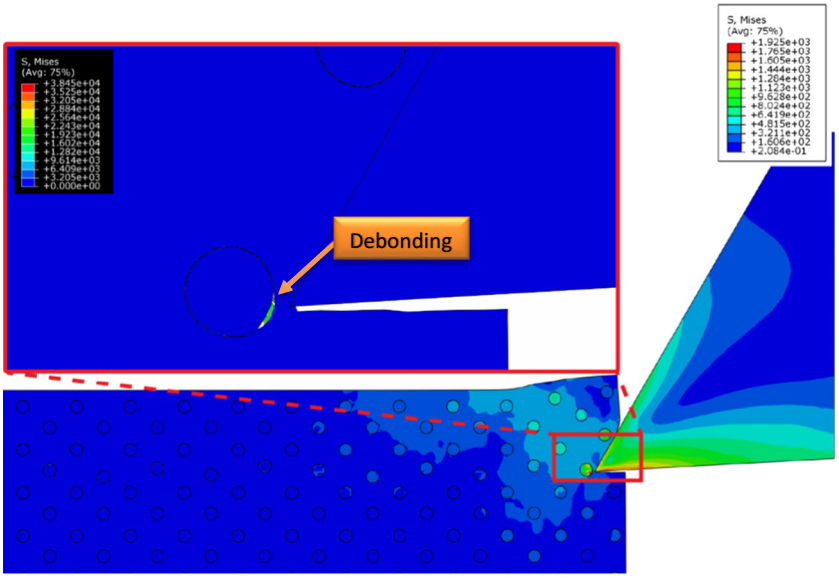

Fig. 5 Interactions between cutting tool and particle located along cutting line (Al 6061/10 % 15 μm Al_2O_3, v=85 m/min, rake angle=30°, width of cut=3 mm)

(a) Stress (MPa) distribution during cutting tool engagement which results in particle debonding

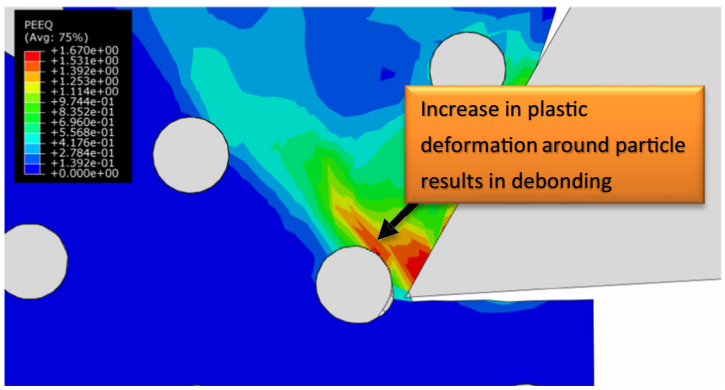

(b) Distribution of equivalent plastic strain around the debonded particle

attributed to the plastic deformations in the matrix around the particle. Figure 5b shows the distribution of equivalent plastic strain around the debonded particle, where an increase in matrix plastic strain in the vicinity of the particle is observed.

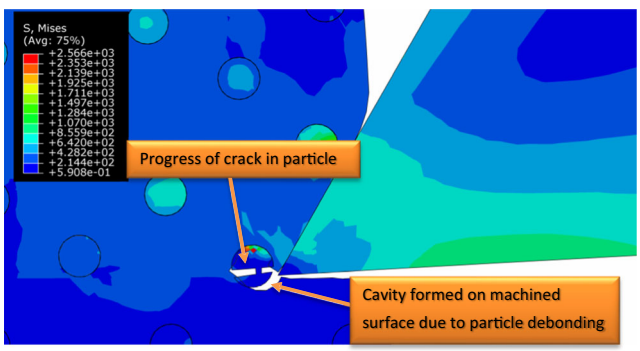

Fig. 6 Stress (MPa) distribution during initiation and growth of crack in the particle (Al 6061/10 % 15 μm Al_2O_3, v=85 m/min, rake angle=30°, width of cut=3 mm)

As the tool continues moving along its path, initiation and development of cracks become visible in the particle which is demonstrated in Fig. 6. Moreover, it is evident in this figure that as a result of debonding, cavities will be formed on the surface, which will consequently deteriorate the machined surface quality.

Figure 7a shows the interaction between the cutting tool and a particle located slightly above the cutting line. In this case, the particle is debonded from the workpiece but stays in the chip material. The stress distribution on the particle shows how the particle is pushed against the matrix material into the chip as a result of interaction with the cutting tool. This can be better understood by studying the pressure stress distribution as depicted in Fig. 7b. In this figure, the increase in pressure on the particles that are being forced into the chip material is evident.

In Fig. 8, stress distribution during the interaction between the cutting tool and a particle located below the cutting line is

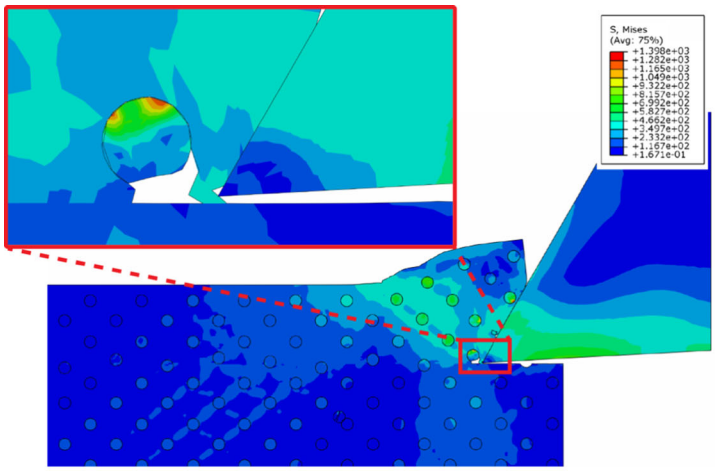

(a) Stress (MPa) distribution during debonding of the particle while being pushed into the chip

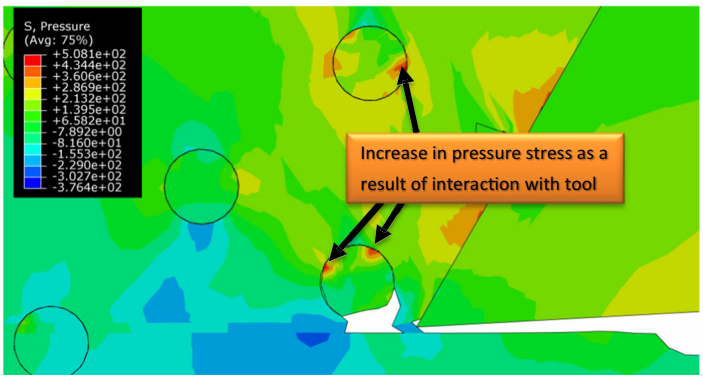

(b) Pressure stress (MPa) distribution during debonding of the particle

Fig. 7 Interactions between cutting tool and particle located above the cutting line (Al 6061/10 % 15 μm Al_2O_3, v= 85 m/min, rake angle=30°, width of cut=3 mm)

shown. It is clear that in spite of the fracture of a small portion of the particle, the larger part of the particulate reinforcement stays bonded to the workpiece material. As a result, a massive increase in surface roughness will not be expected in this scenario. Figure 8 also shows particles embedded in the chip during cutting MMC.

In order to better analyze the scenarios of interactions between the cutting tool and reinforcements, the plastic

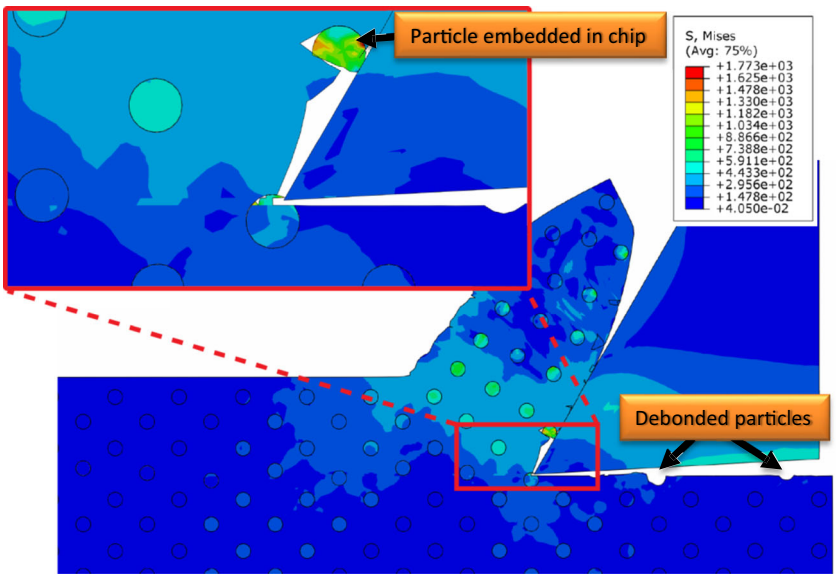

Fig. 8 Stress (MPa) distribution during crack propagation in a particle located below the cutting line (Al 6061/10 % 15 μm Al_2O_3, v=85 m/min, rake angle=30°, width of cut=3 mm)

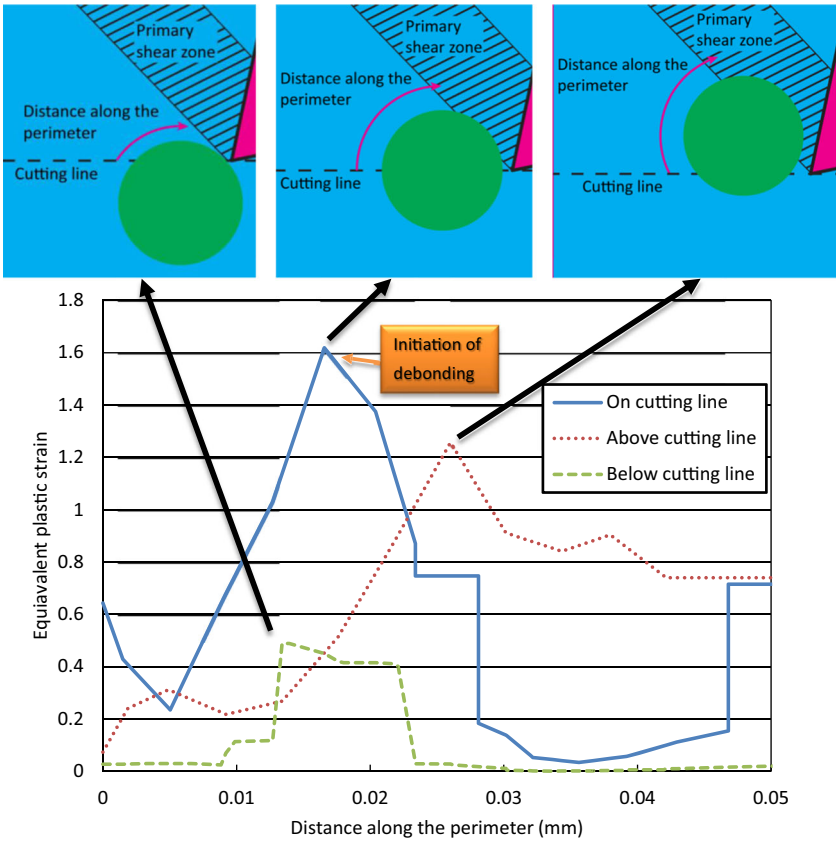

Fig. 9 Equivalent plastic strain in the matrix material versus distance along the perimeter around the particle for various tool-particle interaction scenarios (Al 6061/10 % 15 μm Al_2O_3, v= 85 m/min, rake angle=30°, width of cut=3 mm)

deformation in the matrix material around the particles is studied. Figure 9 shows the plastic strain in the matrix material around the particle versus distance along the particle perimeter. This graph is plotted for the three cases of the particle lying on, below, or above the cutting line. It is evident in this graph that high plastic deformation in the matrix material adjacent to the reinforcement can cause debonding; the plastic strain around the particle on the cutting line is the highest which results in immediate debonding. On the other hand, the low plastic strain around the particle below the cutting line means that the particle stays bonded to the matrix.

Figure 9 also clarifies the relation between particle location with respect to the primary shear zone and plastic deformation around the particle. It is clear in this figure that peaks of plastic deformation around the particle are observed in the primary shear zone.

The knowledge regarding tool-particle interactions presented in this research is a great asset in studying the MMC machining system. This knowledge can only be achieved by means of a comprehensive finite element model which simulates all phases of a real composite. Hence, the developed FE model is considered to be a step forward in understanding MMC cutting process.

4 Conclusion

A micro-mechanical finite element model for simulating the particle-tool interactions during machining of aluminum metal matrix composites was presented in this paper. The presented thermal-displacement model included three distinct phases including the matrix, particles, and the particle-matrix interface. Thermal-elastic-plastic failure models along with cohesive zone models were adopted and utilized for simulation of material behavior. The model predictions were validated through comparison with experimentally measured data. The model's capability to simulate the behavior of all phases of the real composite material during cutting has made it possible to successfully simulate the particle debonding and fracture during cutting process. The model was also used to study different scenarios of the interactions between the cutting tool and particles along the cutting line. The analyses of the simulation have provided a more comprehensive understanding of the machining process of particle-reinforced metal matrix composites.

Acknowledgements The authors acknowledge the support from the National Plan for Science, Technology and Innovation (MARRIFAH),

King Abdulaziz City for Science and Technology, Kingdom of Saudi Arabia, (project number: 13-ADV-971-02).

References

1. Bandyopadhyay NR, Ghosh S, Basumallick A (2007) New generation metal matrix composites. Mater Manuf Process 22(6):679–682
2. Kannan S, Kishawy H (2008) Tribological aspects of machining aluminium metal matrix composites. J Mater Process Technol 198(1):399–406
3. Krishnaraj V, Prabukarthi A, Ramanathan A, Elanghovan N, Kumar MS, Zitoune R, Davim JP (2012) Optimization of machining parameters at high speed drilling of carbon fiber reinforced plastic (CFRP) laminates. Compos Part B 43(4):1791–1799
4. Zitoune R, Krishnaraj V, Sofiane Almabouacif B, Collombet F, Sima M, Jolin A (2012) Influence of machining parameters and new nano-coated tool on drilling performance of CFRP/Aluminium sandwich. Compos Part B 43(3):1480–1488
5. Muguthu JN, Gao D (2013) Profile fractal dimension and dimensional accuracy analysis in machining metal matrix composites (MMCs). Mater Manuf Process 28(10):1102–1109. doi:10.1080/10426914.2013.823501
6. Sidhu SS, Batish A, Kumar S (2013) EDM of metal matrix composite for parameter design using lexicographic goal programming. Mater Manuf Process 28(4):495–500. doi:10.1080/10426914.2013.763958
7. Kishawy HA, Kannan S, Balazinski M (2004) An energy based analytical force model for orthogonal cutting of metal matrix composites. CIRP Ann Manuf Technol 53(1):91–94. doi:10.1016/S0007-8506(07)60652-0
8. Sikder S, Kishawy HA (2012) Analytical model for force prediction when machining metal matrix composite. Int J Mech Sci 59(1):95–103. doi:10.1016/j.ijmecsci.2012.03.010
9. Kishawy HA, Kannan S, Balazinski M (2005) Analytical modeling of tool wear progression during turning particulate reinforced metal matrix composites. CIRP Ann—Manuf Technol 54(1):55–58. doi:10.1016/S0007-8506(07)60048-1
10. Kannan S, Kishawy HA (2006) Surface characteristics of machined aluminium metal matrix composites. Int J Mach Tools Manuf 46(15):2017–2025. doi:10.1016/j.ijmachtools.2006.01.003
11. Bhatnagar N, Nayak D, Singh I, Chouhan H, Mahajan P (2004) Determination of machining-induced damage characteristics of fiber reinforced plastic composite laminates. Mater Manuf Process 19(6):1009–1023
12. Singh G, Teli M, Samanta A, Singh R (2013) Finite element modeling of laser-assisted machining of AISI D2 tool steel. Mater Manuf Process 28(4):443–448
13. Atlati S, Haddag B, Nouari M, Zenasni M (2014) Thermomechanical modelling of the tool-workmaterial interface in machining and its implementation using the ABAQUS VUINTER subroutine. Int J Mech Sci 87:102–117
14. Salahshoor M, Guo YB (2014) Finite element simulation and experimental validation of residual stresses in high speed dry milling of biodegradable magnesium-calcium alloys. Int J Mech Sci 80:153–159
15. Zhu Y, Kishawy HA (2005) Influence of alumina particles on the mechanics of machining metal matrix composites. Int J Mach Tools Manuf 45(4–5):389–398. doi:10.1016/j.ijmachtools.2004.09.013
16. Pramanik A, Zhang LC, Arsecularatne JA (2007) An FEM investigation into the behavior of metal matrix composites: tool-particle interaction during orthogonal cutting. Int J Mach Tools Manuf 47(10):1497–1506
17. Zhou L, Huang ST, Wang D, Yu XL (2011) Finite element and experimental studies of the cutting process of SiCp/Al composites with PCD tools. Int J Adv Manuf Technol 52(5–8):619–626. doi:10.1007/s00170-010-2776-2
18. Dandekar CR, Shin YC (2009) Multi-step 3-D finite element modeling of subsurface damage in machining particulate reinforced metal matrix composites. Compos A: Appl Sci Manuf 40(8):1231–1239
19. Wang T, Xie L, Wang X (2015) Simulation study on defect formation mechanism of the machined surface in milling of high volume fraction SiCp/Al composite. Int J Adv Manuf Technol:1–10. doi:10.1007/s00170-015-6876-x
20. Umer U, Ashfaq M, Qudeiri JA, Hussein HMA, Danish SN, Al-Ahmari AR (2015) Modeling machining of particle-reinforced aluminum-based metal matrix composites using cohesive zone elements. Int J Adv Manuf Technol:1–9. doi:10.1007/s00170-014-6715-5
21. Özel T (2006) The influence of friction models on finite element simulations of machining. Int J Mach Tools Manuf 46(5):518–530
22. Dandekar CR, Shin YC (2012) Modeling of machining of composite materials: a review. Int J Mach Tools Manuf 57:102–121
23. Johnson GR, Cook WH (1983) A constitutive model and data for metals subjected to large strains, high strain rates and high temperatures. In: International Ballistics Committee, The Hague, Netherlands. p 1–2
24. Johnson GR, Cook WH (1985) Fracture characteristics of three metals subjected to various strains, strain rates, temperatures and pressures. Eng Fract Mech 21(1):31–48
25. Shackelford JF, Alexander W (2000) CRC Materials Science and Engineering Handbook, Third Edition. Taylor & Francis
26. Holt JM, Gibson C, Ho CY (1999) Structural alloys handbook. vol v. 2. CINDAS/Purdue University, West Lafayette
27. Lesuer DR, Kay GJ, LeBlanc MM (1999) Modeling large-strain, high-rate deformation in metals. In: Third Biennial Tri-Laboratory Engineering Conference on Modeling and Simulation, Pleasanton, CA, United States of America
28. Munro RG (1997) Evaluated material properties for a sintered α-alumina. J Am Ceram Soc 80(8):1919–1928
29. Foulk JW, Allen DH, Helms KLE (2000) Formulation of a three-dimensional cohesive zone model for application to a finite element algorithm. Comput Methods Appl Mech Eng 183(1–2):51–66. doi:10.1016/S0045-7825(99)00211-X
30. Tvergaard V (2003) Debonding of short fibres among particulates in a metal matrix composite. Int J Solids Struct 40(25):6957–6967. doi:10.1016/S0020-7683(03)00347-0
31. Abaqus (2014) Abaqus 6.14 Documentation. SIMULIA, United States of America